PAPER

Check for updates

Five Co(II) coordination polymers with different counter anions based on [3,5-di(4H-1,2,4-triazol-4-yl)benzoato]− ligand: directed synthesis, structures and magnetic properties†

Wen-Hong Jiang,[a] Han-Zhong Zhang,[a] Guang-Feng Hou,[b] Dong-Sheng Ma,[a] Bin Liu[a] and Ying-Hui Yu [ID] *[a]

As a continuing challenge to obtain the desired coordination polymers in the synthesis stage, the counter ions, the metal–ligand ratio and the involvement of template have great impact on their structure construction and crystal growth. In this paper, three different crystals of coordination polymers **1–3** {{[CoL(μ₂-OH)]}ₙ (**1**), {[CoL₂(H₂O)]·H₂O}ₙ (**2**), {[Co₃L₃(H₂O)]·3NO₃·4H₂O}ₙ (**3**) {L = [3,5-di(4H-1,2,4-triazol-4-yl)benzoate]−} were obtained in one pot with HL and Co(NO₃)₂. By tuning the reactants ratio and employing different templates, each complex could also be synthesized separately. Single-crystal X-ray analyses show that complex **1** exhibited a two-dimensional (2D) layered gek2 net structure. Complex **2** with deprotonated [L]− has two dimensional (2D) nets structure with 3,5L66 topology. Complex **3** displays a new 5,5,6,6-connected three-dimensional (3D) topological network with a point symbol of $(4^{10} \cdot 6^5)(4^5 \cdot 6^5)_2(4^7 \cdot 6^3)_2(4^8 \cdot 6^7)$. When the reactant Co(NO₃)₂ was changed to CoCl₂ or CoSO₄, **4** and **5** {{[CoL(Cl)]·H₂O}ₙ (**4**) and {[Co₂L₂(SO₄)(H₂O)]·2H₂O}ₙ (**5**)} was formed with a similar structure to that of **1**. Complexes **4** and **5** are two-dimensional (2D) frameworks with 4,6L26 topology. Five complexes have been characterized by elemental analysis, infrared spectroscopy, powder X-ray diffraction and thermogravimetry measurements. The magnetic properties of **1–5** are also investigated. The magnetic property investigation reveals that complex **1** exhibits frequency-dependent behavior.

1. Introduction

As an emerging class of tunable hybrid materials, metal organic coordination polymers have been extensively explored not only for their aesthetics of crystalline structures[1] but also for their promising functional purposes, such as storage,[2] photoluminescence,[3] separation,[4] molecular magnetism,[5] catalysis,[6] sensor,[7] ion exchange[8] and optical device[9] etc. Although much of initial interest and enthusiasm have been devoted to their design and synthesis, it remains to be a distant prospects to the rational construction of the expected architectures with desired properties, representing an ambitious goal for chemists. The difficulty in controlling the synthesis of complexes with well-defined architectures and associated functions owes to the influence of many factors, such as solvent system,[10] ratio of the reactants,[11] pH value of reaction mixture,[12] anion,[13] temperature,[14] and reagent concentration[15] etc.

As an important role to maintain charge balance of the complex, the counter ion could greatly influence the topology and dimensionality of the complex, as the coordinated counter ion with a bridging mode could further extend the arrangement of metal node.[16] Meanwhile, templates and molar ratio between the metal salt and the ligand also have an impact on the construction of final structures. Varied reactant ratios and the involvement of templates may perturb the equilibrium of the coordination reaction, thus affecting the crystal formation and eventually leading to a different structure.[17] Further exploring the correlations between the counter anions, the ratio of reactants and template with the topological structures could be helpful for better understanding the self-assemble process in coordination polymers.

Therefore, a judicious selection of functional ligands is important for deliberately achieving structural changes and the functional properties of these coordination polymers.[18] Multi-carboxylic ligands with suitable spacers, especially benzoic acid-based ligands, the 1,2,4-triazole ligand and its derivatives are frequent choices for metal organic networks.[19] As one of ongoing research in our laboratory, the coordination chemistry of a bifunctional ligand which combined with the triazole and carboxylate group have been continuously studied in our group.[20] In this paper, [3,5-di(4H-1,2,4-triazol-4-yl)benzoate]− is

ᵃSchool of Chemistry and Materials Science, Heilongjiang University, Harbin 150080, PR China. E-mail: yuyinghui@hlju.edu.cn; Fax: +86-451-86609151

ᵇAgricultural College, Heilongjiang University, Harbin 150080, PR China

adopted as a building block for the construction of coordination polymers based on cobalt salts with different counter ions. Five new coordination polymers $\{[CoL(\mu_2\text{-OH})]\}_n$ (1), $\{[CoL_2(H_2O)]\cdot H_2O\}_n$ (2), $\{[Co_3L_3(H_2O)]\cdot 3NO_3\cdot 4H_2O\}_n$ (3), $\{[CoL(Cl)]\cdot H_2O\}_n$ (4) and $\{[Co_2L_2(SO_4)(H_2O)]\cdot 2H_2O\}_n$ (5) were successfully synthesized and characterized by single-crystal X-ray diffraction analysis, elemental analysis, IR analysis and thermal gravimetric analysis. The magnetic properties of 1–5 are also investigated. Magnetic investigation for complex 1 indicates that 1 demonstrates frequency-dependent magnetic behavior.

2. Experimental section

2.1 Materials and measurements

All chemicals purchased of reagent grade are used as received without further purification. The ligand 3,5-di(4H-1,2,4-triazol-4-yl)benzoic acid (HL) was synthesized according to the literature.[20] Elemental analyses of C, H, N were processed on a Perkin-Elmer 2400 elemental analyzer. The IR spectra were obtained by using KBr disks on a Perkin-Elmer Spectrum 100 FT-IR spectrometer equipped with a DGTS detector (32 scans) in the range of 4000 to 500 cm^{-1}. A Perkin-Elmer STA 6000 was used for thermal analyses under air atmosphere, with a heating rate of 10 °C min^{-1} in a temperature range from 50 to 800 °C. Bruker-D8 Advance X-ray diffractometer with Cu-Kα radiation (λ = 1.5406 Å) was employed for powder X-ray diffraction (PXRD) analysis. The magnetic susceptibility for complexes 1–5 were measured with a Quantum Design MPMS XL-7 SQUID-VSM magnetometer. The magnetic corrections were made by using Pascal's constants.

2.2 Syntheses of 1–5

2.2.1 Synthesis of $\{CoL(\mu_2\text{-OH})\}_n$ (1). A mixture of CoCO$_3$ (11.9 mg, 0.1 mmol), HL (25.6 mg, 0.1 mmol) and imidazole (6.8 mg, 0.1 mmol) as template in 5 mL H$_2$O and 5 mL EtOH (95%) was sealed in a 16 mL Teflon lined stainless steel container and heated at 160 °C for 3 days. After cooling to room temperature at a rate of 5 °C h^{-1}, brown yellow block crystals were picked out and washed with distilled water. Anal. calcd for C$_{11}$H$_8$CoN$_6$O$_3$ (331.16): C, 39.89; H, 2.44; N, 25.37; found: C, 39.75; H, 2.58; N, 25.54. IR (KBr pellet, cm^{-1}) 1: 3281 (m), 3072 (m), 2975 (w), 2932 (w), 2873 (w), 2366 (w), 2319 (w), 1692 (s), 1645 (s), 1541 (s), 1512 (s), 1455 (m), 1413 (m), 1382 (m), 1270 (s), 1223 (s), 1161 (s), 1110 (m), 1013 (m), 930 (m), 845 (m), 746 (m), 700 (s), 669 (m), 525 (m), 422 (w).

2.2.2 Synthesis of $\{[Co(L)_2(H_2O)]\cdot H_2O\}_n$ (2). A mixture of Co(NO$_3$)$_2$ (58.2 mg, 0.2 mmol) and HL (25.6 mg, 0.1 mmol) in 5 mL H$_2$O and 5 mL EtOH (95%) was sealed in a 16 mL Teflon lined stainless steel container and heated at 160 °C for 3 days. After cooling to room temperature, red needle crystals of 2 was obtained after filtration. Anal. 2 calcd for (C$_{22}$H$_{18}$N$_{12}$O$_{16}$Co) (605.41) C, 43.64%; H, 3.00%; N, 27.75%; found: C, 43.48%; H, 3.16%; N, 27.97%. IR (KBr pellet, cm^{-1}) 2: 3515 (m), 3132 (m), 3080 (s), 3018 (m), 2963 (m), 2357 (w), 2336 (w), 1584 (s), 1522 (s), 1408 (s), 1367 (s), 1221 (m), 1209 (m), 1100 (s), 1055 (s), 871 (m), 793 (m), 761 (m), 717 (m), 680 (w), 634 (m), 587 (w).

2.2.3 Synthesis of $\{[Co_3L_3(H_2O)]\cdot 3NO_3\cdot 4H_2O\}_n$ (3). A mixture of Co(NO$_3$)$_2$ (29.1 mg, 0.1 mmol), HL (25.6 mg, 0.1 mmol) and adding 1,3,5-benzenetricarboxylic acid (21.0 mg, 0.1 mmol) as template in 5 mL H$_2$O and 5 mL EtOH (95%) was sealed in a 16 mL Teflon lined stainless steel container and heated at 160 °C for 3 days. After cooling to room temperature at a rate of 5 °C h^{-1}, red crystals of 3 were obtained after filtration. Anal. calcd for C$_{33}$H$_{31}$N$_{21}$O$_{20}$Co$_3$ (1218.58): C, 32.52%; H, 2.57%; N, 24.13%; found: C, 32.30%; H, 2.75%; N, 24.31%. IR (KBr pellet, cm^{-1}): 3281 (m), 3065 (w), 2979 (w), 2936 (w), 2875 (w), 2362 (w), 2324 (w), 1689 (s), 1647 (s), 1543 (s), 1509 (m), 1456 (m), 1413 (w), 1388 (w), 1275 (m), 1248 (m), 1222 (m), 1201 (m), 1159 (m), 1111 (m), 1037 (w), 1018 (w), 934 (w), 920 (w), 840 (w), 748 (w), 700 (m), 670 (w), 521 (w), 417 (w), 354 (w).

2.2.4 Synthesis of $\{[CoL(Cl)]\cdot H_2O\}_n$ (4). The complex was obtained by the same procedure used for preparation of 2 except that CoCl$_2$ (23.7 mg, 0.1 mmol) was used instead of Co(NO$_3$)$_2$ (58.2 mg, 0.2 mmol). Red cubic crystals of 4 was obtained by filtration was wash by water. Anal. calcd for C$_{11}$H$_9$N$_6$O$_3$CoCl (367.62): C, 35.94%; H, 2.47%; N, 22.85%; found: C, 35.66%; H, 2.62%; N, 23.01%. IR (KBr pellet, cm^{-1}): 3613 (m), 3518 (m), 3057 (m), 3011 (m), 2358 (w), 2337 (w), 1619 (s), 1601 (s), 1540 (m), 1405 (w), 1341 (s), 1313 (s), 1240 (m), 1214 (m), 1107 (m), 1077 (m), 1037 (m), 897 (w), 788 (m), 770 (m), 728 (s), 692 (m), 669 (m), 642 (m), 554 (m), 528 (w).

2.2.5 Synthesis of $\{[Co_2L_2(SO_4)(H_2O)]\cdot 2H_2O\}_n$ (5). The complex was obtained by the same procedure used for preparation of 2 except that CoSO$_4$ (28.1 mg, 0.1 mmol) was used instead of Co(NO$_3$)$_2$ (58.2 mg, 0.2 mmol). Orange cubic crystals of 5 was obtained by filtration. Anal. calcd for (C$_{22}$H$_{20}$N$_{12}$O$_{11}$Co$_2$S) (778.42): C, 33.94%; H, 2.08%; N, 21.58%; found: C, 33.72%; H, 2.24%; N, 21.70%; IR (KBr pellet, cm^{-1}): 3422 (m), 3060 (m), 3017 (m), 2358 (w), 2340 (w), 1896 (w), 1617 (s), 1543 (m), 1406 (w), 1348 (s), 1317 (m), 1219 (m), 1149 (m), 1113 (m), 1081 (m), 1030 (m), 895 (m), 793 (m), 765 (w), 731 (s), 694 (m), 672 (w), 639 (m), 626 (w), 555 (w).

2.2.6 One pot synthesis of 1, 2 and 3. A mixture of Co(NO$_3$)$_2$ (29.1 mg, 0.1 mmol) and HL (25.6 mg, 0.1 mmol) in 5 mL H$_2$O and 5 mL EtOH (95%) was sealed in a 16 mL Teflon lined stainless steel container and heated at 160 °C for 3 days. After cooling to room temperature, crystals of 1, 2 and 3 was obtained after filtration.

2.3 X-ray crystallography

Single-crystal X-ray diffraction data for complexes 1–5 were collected on a Rigaku R-AXIS RAPID imaging plate diffractometer with graphite-monochromated Mo Kα (λ = 0.71073 Å) at 291 K. Empirical absorption corrections based on equivalent reflections were applied. The structures of complexes 1–5 were solved by direct methods and refined by full-matrix least-squares methods on F^2 with SHELXS-97 crystallographic software package.[21] All the hydrogen atoms of ligands HL in complexes 1–5 were generated geometrically. The water molecules in 2, 3, 5 were located directly. The crystal parameters, data collection and refinement results for complexes 1–5 are summarized in Table 1. Selected bond lengths and angles of complexes 1–5 are listed in Table S1† and the H-bond lengths and angles are shown in Table S2† (see

Table 1 Crystallographic data for complexes **1–5**[a]

Crystal parameters	1	2	3	4	5
Empirical formula	$C_{11}H_8N_6O_3Co$	$C_{22}H_{18}N_{12}O_6Co$	$C_{33}H_{31}N_{21}O_{20}Co_3$	$C_{11}H_9N_6O_3CoCl$	$C_{22}H_{20}N_{12}O_{11}Co_2S$
Formula weight	331.16	605.41	1218.58	367.62	778.42
Crystal system	Orthorhombic	Monoclinic	Monoclinic	Orthorhombic	Orthorhombic
Space group	*Cmcm*	*P2₁/c*	*C2/c*	*Pmma*	*Pmm2*
a (Å)	21.9686	16.8418(4)	16.9247(4)	7.1293(14)	6.9023(2)
b (Å)	6.8017	7.0186(2)	17.5262(4)	11.442(2)	11.6321(4)
c (Å)	20.0238	19.1189(4)	15.1234(4)	8.2387(16)	8.0322(3)
α (°)	90	90	90	90	90.00
β (°)	90	101.871(2)	93.431(2)	90	90.00
γ (°)	90	90	90	90	90.00
V (Å³)	2992.0(2)	2211.63(9)	4477.95(19)	672.1(2)	644.89(4)
Z	8	4	4	2	1
D_{caled} (Mg cm⁻³)	1.470	1.818	1.808	1.817	2.004
μ (mm⁻¹)	1.165	0.851	1.205	1.498	1.459
Collected/unique	3119/1393	9165/3886	8411/3931	5072/680	1826/1114
R_{int}	0.0252	0.0270	0.0313	0.0346	0.0245
GOF on F^2	1.032	1.041	1.042	1.078	1.023
R ($I > 2\sigma(I)$)	$R_1 = 0.0539$	$R_1 = 0.0373$	$R_1 = 0.0599$	$R_1 = 0.0297$	$R_1 = 0.0341$
	$wR_2 = 0.1785$	$wR_2 = 0.0894$	$wR_2 = 0.1525$	$wR_2 = 0.0784$	$wR_2 = 0.0304$
R (all data)	$R_1 = 0.0723$	$R_1 = 0.0515$	$R_1 = 0.0865$	$R_1 = 0.0325$	$R_1 = 0.0736$
	$wR_2 = 0.1957$	$wR_2 = 0.0968$	$wR_2 = 0.1673$	$wR_2 = 0.0803$	$wR_2 = 0.0700$

[a] $R_1 = (\Sigma|F_o| - |F_c|)/\Sigma|F_o|$. $wR_2 = [\Sigma w(F_o^2 - F_c^2)^2/\Sigma w(F_o^2)^2]^{1/2}$.

the ESI†). Crystallography data have been deposited to the Cambridge Crystallography Data Centre with deposition numbers CCDC: 1528099–1528103 for **1–5**.†

3. Results and discussion

3.1 Crystal structure description of 1

Crystallographic analysis reveals that complex **1** crystallizes in the orthorhombic space group *Cmcm*. Each asymmetric unit contains one crystallographic independent Co(II), one [L]⁻ and one μ₂-bridging hydroxyl groups (Fig. 1a). Each Co(II) is coordinated by four triazole nitrogen atoms (N2, N2[II], N3[III], and N3[IV]) and two μ₂-bridging hydroxyl groups (O2 and O2[V]). Thus the coordination environment of Co(II) atom could be described as a octahedral geometry with N_4O_2 donor set. The Co1–N bond lengths are from 2.189(5) Å to 2.196(1) Å, the Co1–O ones are 1.989(7) Å and 1.995(0) Å, respectively. The coordinated hydroxyl groups connect Co(II) cations to form chains along
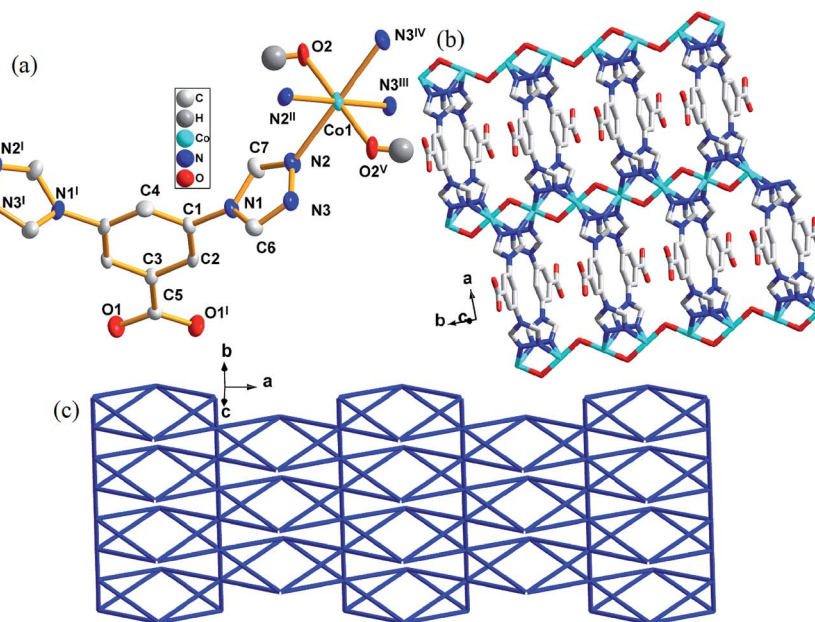

Fig. 1 (a) Coordination environment of Co(II) atom in complex **1**, the H-atoms were omitted for clarity. (b) 2D supramolecular structure of **1**. (c) Schematic illustrating topology of the bimodal (4,6)-connected net of complex **1**. Symmetry code: I = 2 − *x*, *y*, *z*; II = *x*, *y*, 1.5 − *z*; III = 1.5 − *x*, 0.5 + *y*, *z*; IV = 1.5 − *x*, 0.5 + *y*, 1.5 − *z*; V = 1.5 − *x*, −0.5 + *y*, 1.5 − *z*.

[010] direction. The central Co(II) cations further link each chain through N2, N3, N2^I and N3^I atoms of [L]$^-$ along [100] direction, eventually generating a 2D layered structure (Fig. 1b). The distance between two [Co]$^{2+}$ cations is 3.400(9) Å.

A better insight into the structure **1** can be accessed by topological analysis by considering each ligand as a 4-connector and the central Co(II) atom as a 6-connector. Such connectivity repeats infinitely to give a 2D framework, as indicated in Fig. 1b. Analysis of the coordination sequence of **1** shows that its topology is related to gek2 by the TOPOS 4,[22] both the ligand and metal nodes result in a symbol $(3^2 \cdot 4^4)(3^4 \cdot 4^2 \cdot 6^4 \cdot 7^5)$ as shown in Fig. 1c.

3.2 Crystal structure description of 2

Complex **2** crystallizes in monoclinic space group $P2_1/c$. There is one Co(II) atom, two [L]$^-$, one coordinated water molecules and one lattice water molecule in an asymmetric unit of **2** (lattice water molecule was omitted in Fig. 2a). Co1 is six coordinated by two nitrogen atoms from two different triazoles (N6^{II}, N8^{III}), three carboxylate oxygen atoms from three different [L]$^-$ anions (O1, O3, O4^I) and one oxygen atom from one coordinated water molecule (O5), forming a distorted octagonal coordination geometry. The Co1–N bond lengths are 2.135(3) and 2.173(9) Å, the Co1–O ones are in the range of 2.073(7)–2.136(4) Å. O3 and O4 from one ligand linked two Co1 atoms with a distance of 4.990(0) Å between Co–Co.

In complex **2**, N6 and O1 of [L]$^-$ link Co(II) to form a 1D chain along [001] direction. The central Co(II) atoms link O3 and O4 of the ligand to form a 1D chain along [010] direction, the 1D chain further links N8 of the ligand to form a 2D layered

structure along [001] direction. The topological method is also employed to get a better structural insight of **2**. As described above, each Co(II) atom is connected by five ligands, thus it can be considered as a five connector node. The two ligands connecting three or two Co(II) atoms can be regarded as three and two connectors, respectively. Such connectivity repeats infinitely to give a 2D network with a 3,5L66 topology, as schematically shown in Fig. 2c.

3.3 Crystal structures descriptions of 3

Complex **3** crystallizes in monoclinic space group $C2/c$. There is one-half Co atoms, one-half [L]$^-$ anions, a half coordinated water molecule, one-half [NO$_3$]$^-$ anions and two lattice water molecules (solvent molecules were omitted) in an asymmetric unit of **3** (Fig. 3a). The Co1 atom with distorted octahedral coordination geometry is six coordinated by two carboxylate oxygen atoms (O1, O3^{III}) from two different [L]$^-$, one oxygen atom from coordination water molecule (O9) and three triazole nitrogen atoms (N1, N6^I, N9^{II}) from three different [L]$^-$. Co2 is six-coordinated by six triazole nitrogen atom (N2^{II}, N5^{IV}, N8, N2^{VII}, N5^{VI}, N8^V) from six different [L]$^-$ to complete the distorted octahedral coordination geometry.

CoN$_3$O$_3$ and CoN$_6$ SBUs are linked by the ligands to form a 3D structure. The five-connected ligand links Co1 to form 1D chains along [001] direction, which further link Co2 giving rise to a 3D structure in Fig. 3c. The six-connected ligand links Co1 to a 2D layer structure, which further connects Co2 to generate a 3D structure in Fig. 3d. Two kinds of 3D structures are joint together through Co to eventually build the structure shown in Fig. 3e. The basic building block of this structure is the
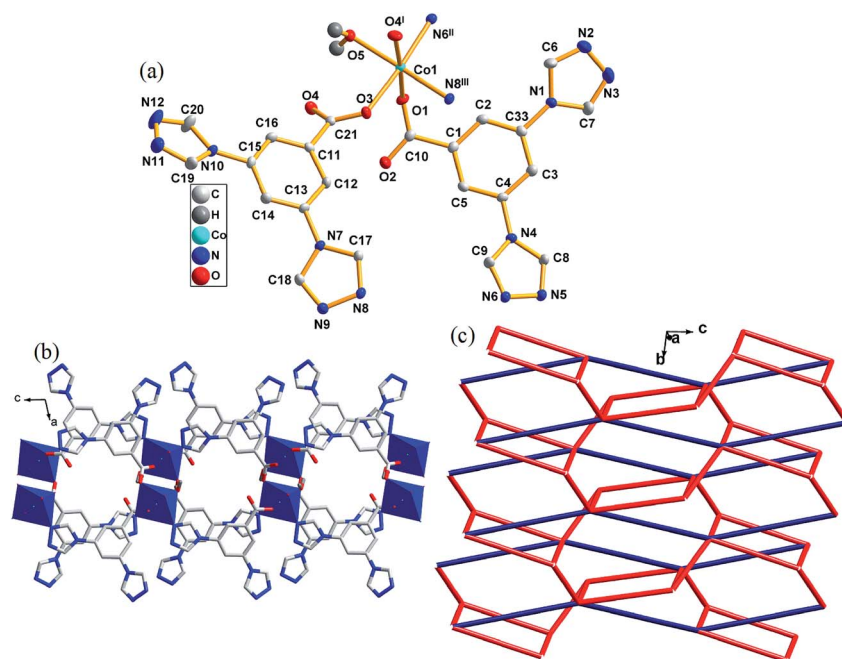

Fig. 2 (a) The coordination environment of Co(II) atom in complex **2**. The hydrogen atoms and the lattice water molecules were omitted for clarity. (b) 2D network in complex **2**. (c) Schematic illustrating topology of 2D supramolecular structure in **2**. Symmetry code: I = 1 − x, 0.5 + y, 0.5 − z; II = x, 1.5 − y, 0.5 + z; III = 1 − x, 2 − y, −z.
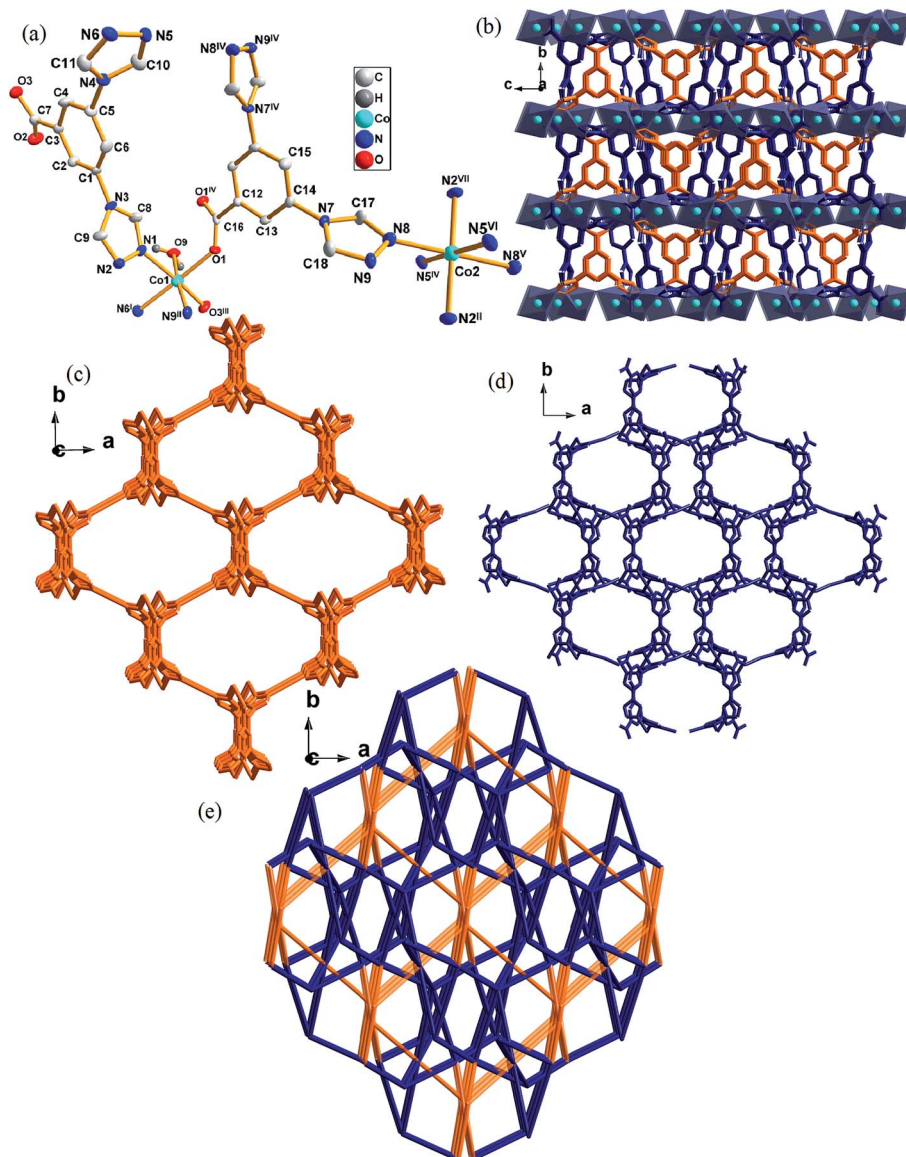
Fig. 3 (a) Coordination environment of Co(II) atom in complex **3**. The hydrogen atoms and solvent molecules were omitted for clarity. (b) 3D network in complex **3**. (c) The six-connected coordination mode of [L]⁻ in complex **3**. (d) The five-connected coordination mode of [L]⁻ in complex **3**. (e) Schematic illustrating topology of complex **3**. Symmetry code: I = 1.5 − x, 0.5 + y, 1.5 − z; II = 2 − x, −y, 1 − z; III = 0.5 + x, 0.5 − y, −0.5 + z; IV = 2 − x, y, 1.5 − z; V = 2.5 − x, −0.5 − y, 1 − z; VI = 0.5 + x, −0.5 − y, −0.5 + z; VII = 0.5 + x, −0.5 + y, z.

dinuclear [Co₂(L)₂]²⁺ entity, in which two [L]⁻ link two metal nodes into a 3D structure with a Co–Co distance of 10.349(1) Å.

From a topological view of structure of **3**, two kinds of Co(II) atoms can be considered as five and six connector nodes and two ligands can be regarded as five or six connectors, respectively. Such connectivity repeats infinitely to give a 3D framework with a point symbol $(4^{10}\cdot6^5)(4^5\cdot6^5)_2(4^7\cdot6^3)_2(4^8\cdot6^7)$.

3.4 Crystal structures descriptions of 4 and 5

When the reactant Co(NO₃)₂ was changed to CoCl₂ or CoSO₄, a similar structure was formed to that of **1**. Complex **4** crystallizes in the orthorhombic space group *Pmma*. There is one Co(II) atom, one [L]⁻, one [Cl]⁻ and one lattice water molecule (lattice water were omitted) in an asymmetric unit of **4** (Fig. 4a). The

Co1 atoms with a distorted octahedral coordination geometry is six coordinated by four nitrogen atoms (N2, N2ᴵⱽ, N2ⱽᴵ, N2ⱽᴵᴵ) from four different [L]⁻ and two [Cl]⁻ (Cl1, Cl1ⱽ). However, complex **5** crystallizes in orthorhombic space group *Pmm*2 (Fig. 4b). The asymmetric unit of **5** contains one crystallographically independent [Co]²⁺ ion, one [L]⁻, a half [SO₄]²⁻, a half coordinated water molecule and one lattice water molecule. Co1 is six-coordinated by four triazole nitrogen atoms (N1, N3, N1ᴵ, N3ᴵ) from four different [L]⁻, one oxygen atom (O1w) from terminal water molecule, one oxygen atom (O3) from [SO₄]²⁻ to complete the distorted octahedral coordination geometry.

In **4**, the [Cl]⁻ connect two Co(II) cations to form chains along [100] direction. The central Co(II) cations further link each chain
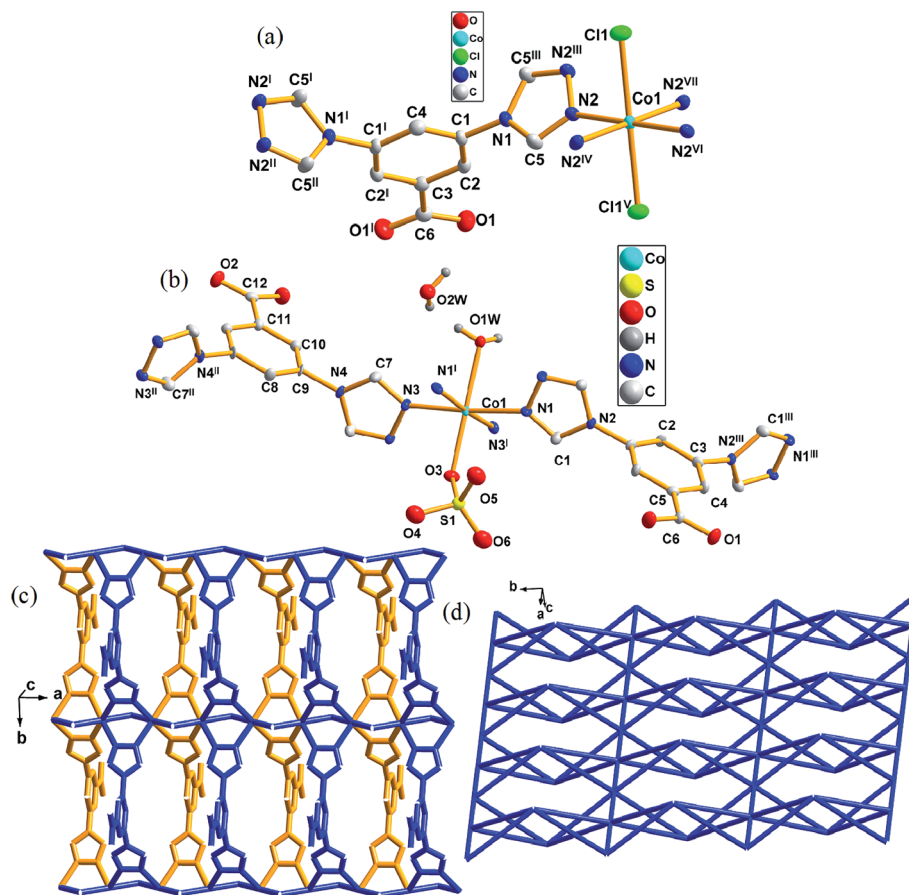
Fig. 4 (a) Coordination environment of Co(ɪɪ) atom in complex **4** (the hydrogen atoms and one lattice water molecules were omitted for clarity). (b) Single molecular structure of complex **5**. The hydrogen atoms were omitted for clarity. (c) Two dimensional layers and its 4,6-connected net for **4** and **5**. (d) Schematic illustration of 2D topological framework in complexes **4** and **5**. Symmetry code for **4**: I = 0.5 − x, 1 − y, z; II = x, 1 − y, z; III = 0.5 − x, y, z; IV = 1 − x, y, 1 − z; V = 0.5 + x, 2 − y, 1 − z; VI = 1 − x, 2 − y, 1 − z; VII = x, 2 − y, z. Symmetry code for **5**: I = x, 1 − y, z; II = 1 − x, −y, z; III = 2 − x, 2 − y, z.
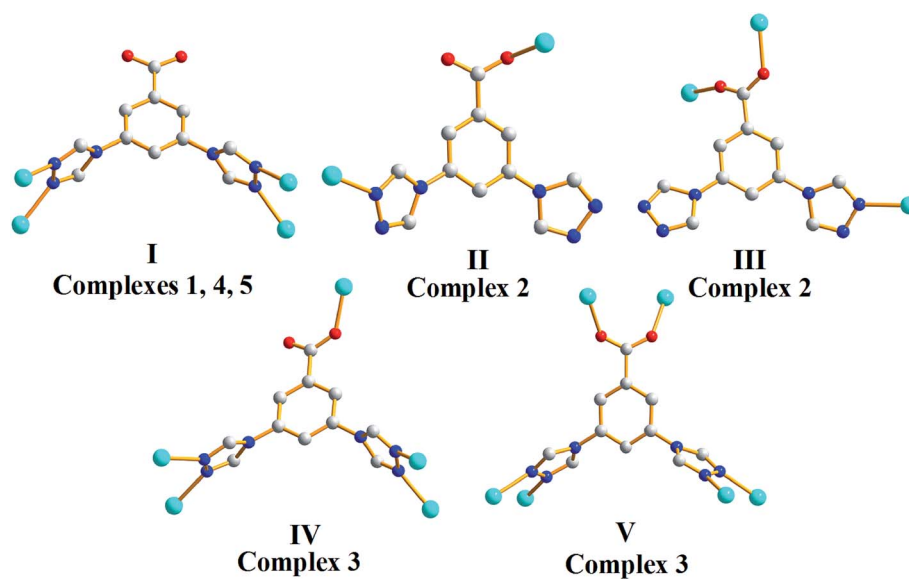

Fig. 5 Five coordination modes of [L]⁻ in complexes **1**–**5**.

through N2, N2^I, N2^{II} and N2^{III} atoms of [L]$^-$ along [010] direction, eventually generating a 2D layered structure (Fig. 4c). The distance between two [Co]$^{2+}$ cations is 3.564(7) Å. In complex **5**, same coordination and connection modes as those in **4** generated same structures, however, the only difference between them was the [Cl]$^-$ anions in **4** changed to oxygen atoms from the coordination water molecule and [SO$_4$]$^{2-}$. In **5**, the distance between two [Co]$^{2+}$ ions are 3.375(9) and 3.526(4) Å.

On the other hand, each [L]$^-$ connects four Co(II) atoms with its two triazole groups. If the coordination linkage between [L]$^-$ was neglected, an infinite 1D chain was obtained via Co–Cl coordination. Each [L]$^-$ links Co atoms to form infinite 1D chains which were further linked by [Cl]$^-$ to give a 2D layer structure (Fig. 4c). According to the simplification principle, the central Co(II) atom could be viewed as a 6-connector and each [L]$^-$ ligand be considered as a 4-connector. The resulting structure of **4** and **5** are a 4,6-connected net with a schläfli symbol 4,6L26 (Fig. 4d).

In **1**, **4** and **5**, different counter anions generate different complexes based on the same central metal Co(II). In **1**, the bond length of Co–O is 1.955(0) Å, that of Co–Cl in **4** is 2.485(3) Å and those of Co–O in **5** are 2.154(9) and 2.251(9) Å, respectively. Meanwhile, different anions also have an influence on the distances between Co–Co. Moreover, same connection modes are present in **1**, **4** and **5**.

3.5 Structures diversity

The selection of suitable ions is an important key factor in the design and synthesis of novel multidimensional coordination polymers with appealing functionality. In this work, we adopted [L]$^-$ and cobalt salts with different anions ([NO$_3$]$^-$, [Cl]$^-$ and [SO$_4$]$^{2-}$) for the construction of coordination polymers. Influenced by different counter anions, **1–5** demonstrate different frameworks based on Co(II) nodes. As illustrated in Fig. 5, HL ligands adopt a total of five types of coordination modes, acting as bi-(**2**), tri-(**2**), tetra-(**1**, **4** and **5**), penta-(**3**) and hexa-dentate(**3**) ligands in **1–5**. All [Co]$^{2+}$ are six connected in complexes **1–5**.

As **1**, **4** and **5** share the same coordination and connection mode, we will mainly discuss the structural differences of **1**, **2** and **3**. Generally, various coordination modes of the ligands provides the possibilities of the formation of versatile structures. In complex **1**, the carboxyl group is not involved in the coordination, two triazoles of the ligand are four connected to form a 2D structure. In complexes **2** and **3**, the carboxyl groups demonstrate both monodentate and bis-monodentate coordination modes. The ligands in **2** exhibit two kinds of coordination mode (II, III). One is two connected, the other one is three connected to form a 2D structure. In **3**, the ligands also have two kinds of coordination mode (IV, V). One is five connected, the other one is six connected to give a 3D structure.

3.6 Directed synthesis of complexes 1, 2 and 3

Among these complexes, **1**, **2** and **3** are originally obtained in one pot by the reaction of Co(NO$_3$)$_2$ and the ligand under solvothermal conditions (Fig. 6a). Afterwards, we successfully fulfilled the directed synthesis for each of them by tuning the ratio between reactants, employing different templates and counter anions. Complex **1** alone could be produced under the same solvothermal reaction conditions except supplying imidazole as template and employing CoCO$_3$ instead of Co(NO$_3$)$_2$, the crystal appearance as shown in Fig. 6b. When tuning the molar ratio between Co(NO$_3$)$_2$ and the ligand to 2 : 1, **2** was obtained separately (Fig. 6c). In the presence of 1,3,5-benzenetricarboxylic acid as template, only the crystals of **3** was achieved (Fig. 6d). From the hundreds of experiments, we found that different reaction conditions including metal salts and templates could not only lead to the production of different complexes mixtures but also have a strong influence on the crystal appearance. The reactant ratio, counter anion and the addition of different templates can impact the complex production with different structures. In our investigation, two different templates imidazole and 1,3,5-benzenetricarboxylic acid were found to play important role in the growth and formation of the crystals. Considering their different effect on
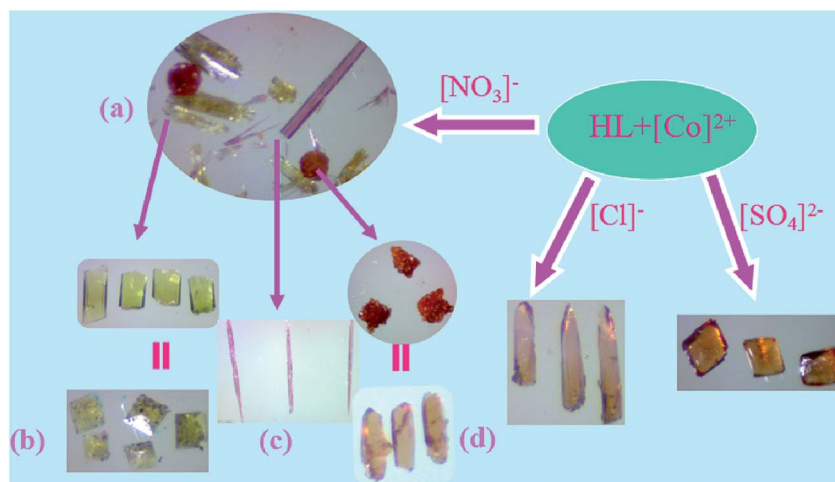

Fig. 6 Crystal morphological comparison of complexes **1–5**.

the solution pH value, we were wondering if different pH value could have such big influence on the reaction. Accordingly, we employed another three polycarboxylic acids 1,4-benzenedicarboxylic, 1,2,3-benzenetricarboxylic acid or 1,2,4,5-benzenetetracarboxylic acid as templates, respectively, to conduct the reaction under the same conditions, however, we obtained mixtures of **1**, **2**, **3** with different quantities. Instead, only the crystals of **3** was achieved with 1,3,5-benzenetricarboxylic acid as template. The results revealed that this phenomenon might not be merely caused by the solution pH, which further confirms the template effect in the synthesis process. In the presence of templates, the synthetic process controls the structure of the complex and is therefore regarded as one way by which the structural characteristics of template molecules are transcribed into the resulting complex. Complexes **1**, **2** and **3** demonstrate different coordination modes resulting in three different structures.

3.7 Thermogravimetric analyses

The TGA measurements of complexes **1–5** were carried out in the temperature range 50–800 °C under atmosphere with a heating rate of 10 °C min^{-1} (Fig. S2†). Complex **1** shows the first weight loss of 5.75% corresponds to the departure of the hydroxyl groups in the range of 50–165 °C (calcd: 5.14%). Then the loss of organic ligands occurs in the range of 165–440 °C, and the remaining weight could be ascribed to CoO (obsd 22.21%, calcd 22.63%). In complex **2**, the decomposition of the framework occurs at the range of 310–573 °C. With the loss of ligand molecule, the remaining weight can be attributed to the formation of CoO (obsd: 11.54%, calcd: 12.38%). For complex **3**, TGA curve displays the first weight loss of 8.01% from 50 to 164 °C corresponding to the departure of lattice water molecules and coordinated water molecules (calcd: 7.39%). The second weight loss occurred from 164 to 440 °C, the remaining weight corresponds to the formation of CoO (obsd: 18.30%; calcd: 18.45%). Complex **4** exhibits the first weight loss of 4.88% at 246 °C which could be ascribed to the loss of lattice water molecule (calcd: 4.90%). Further decomposition from 246 to

675 °C is consistent with the loss of the ligand molecule (obsd: 75.68%; calcd: 74.32%). For complex **5**, the first weight loss of 6.18% occurs at 356 °C corresponding to the release of water molecule (calcd: 6.94%). Further, the second weight loss was observed between 356–612 °C due to the release of ligand molecule. The remaining weight was ascribed to the formation of CoO (obsd: 19.15%; calcd: 19.25%).

3.8 Magnetic property

Magnetic measurements were carried out on crystalline samples of **1–5**, the phase purity of which was confirmed by XRPD (Fig. S3†). Solid-state magnetic susceptibility measurements for **1–5** were performed in the range 1.8–300 K under a field of 1000 Oe.

In complex **1**, a $\chi_M T$ value of 2.70 cm^3 K mol^{-1} is higher than that for a spin-only case (1.87 cm^3 K mol^{-1}, $S = 3/2$) at 300 K, as expected for an orbital contribution.[23] With the lowered temperature, the $\chi_M T$ value keeps decreasing until at *ca.* 35 K and rises to a maximum at 12 K before dropping. Such results indicate the presence of ferromagnetic interaction occurring in cobalt ions of Co–O–Co chains in **1**. Spin–orbit coupling effects and the presence of possible antiferromagnetic interactions explained the decrease of the $\chi_M T$ plot upon cooling at high temperature. Fitting the data above 50 K by the Curie–Weiss law gives $C = 3.60$ cm^3 K mol^{-1} and $\theta = -101.59$ K (Fig. 7). Generally, the single-ion behavior of octahedral Co(ɪɪ) could lead to a bigger negative θ value, however, such a large value could better be explained by the dominant antiferromagnetic coupling between Co(ɪɪ) ions.

In **1**, the Co–O(H)–Co angles range between 117.19°, resulting in competing antiferromagnetic and ferromagnetic interactions. Considering the presence of the numerous magnetic exchange pathways in the chains and the adjacent coordinated octahedrons of the anisotropic Co(ɪɪ) ions that tilt towards each other, it is possible for spin canting occurrence. As the shortest Co···Co distance across the bridge is 3.4009 Å, the magnetic exchange coupling through these bridges is expected to be very
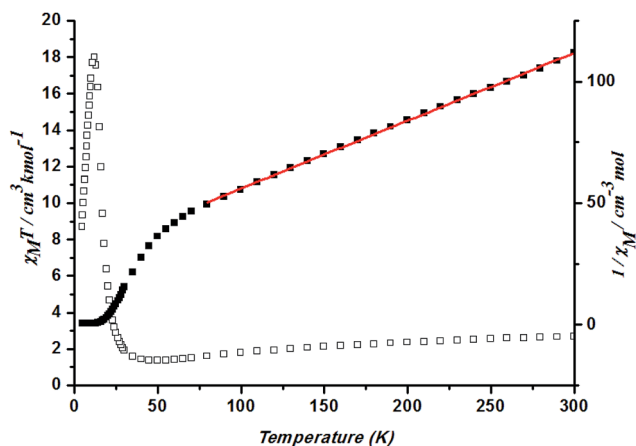

Fig. 7 Plots of $\chi_M T$ *vs. T* for **1** and the temperature dependence of 1/χ_M, the best fit of the curve (red) to the Curie–Weiss law.
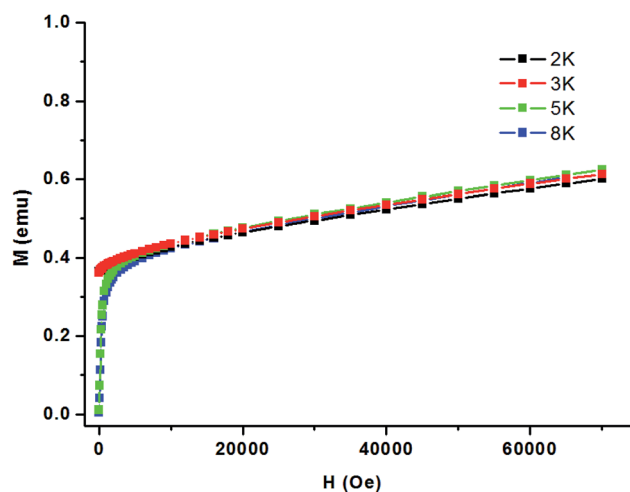

Fig. 8 Magnetization *M versus* the magnetic field *H* for **1** at different low temperatures.
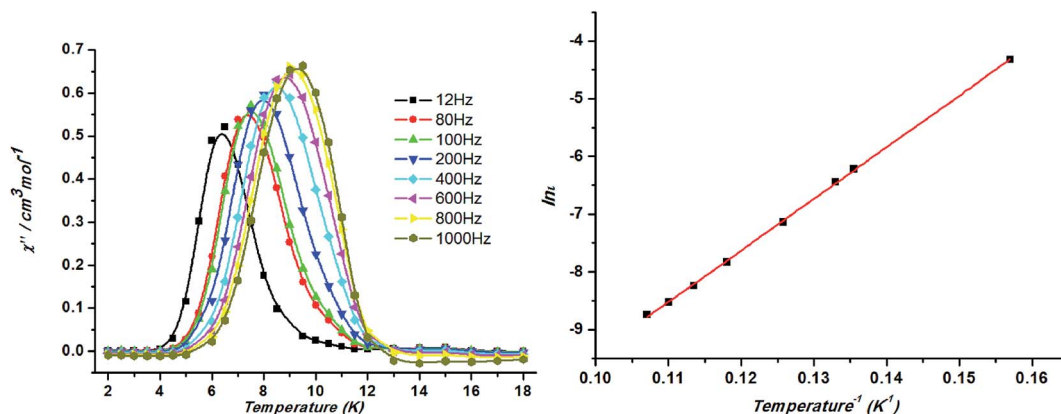
Fig. 9 Frequency dependence of the out-of-phase ac susceptibility (χ'') between 12 and 1000 Hz at $H_{dc} = 0$ Oe for **1** (left). Relaxation time of the magnetization $\ln(\tau)$ vs. T^{-1} (Arrhenius plot using ac data) for **1**. The line corresponds to the fit(right).

weak in **1**. Fig. 8 shows an sudden increase to above 0.38 Nβ of magnetization below 2500 Oe and then increases linearly to 0.61 Nβ at 70 kOe without achieving saturation, which suggests the canted antiferromagnetism of **1**. This could be further confirmed by the field dependence of magnetization at 2 K. The isonic anions between the Co(II) ions from neighboring chains could only lead to very weak magnetic interactions.

Temperature dependent alternating-current (ac) magnetic susceptibilities of **1** is obtained at zero direct-current (dc) fields to further understand the low-temperature magnetic properties of **1**. Slow magnetic relaxation was found to be present in **1**, considering the frequency-dependent behaviors of in-phase (χ'_M) and out-of-phase (χ''_M) components of the susceptibilities below ca. 12 K (ref. 24) (Fig. 9, left). Plotting $\ln \tau$ against $1/T$ has been fitted following the Arrhenius equation $\tau = \tau_0 \exp(\Delta E/k_B T)$ (τ is the relaxation time). The calculated τ_0 (1.05×10^{-8} s) and ΔE (89.5 K) suggests that the slow relaxation of magnetization in **1** is a thermally activated process (ΔE is the energy barrier to reverse the magnetization). The ΔE and τ_0 values are in the normal range for superparamagnets including SCMs (10^{-6} to 10^{-13} s)[25] (Fig. 9, right). The strong frequency dependence of the relaxation time and the physically reasonable value of τ_0, without introducing any scaling factor, rule out the possibility that the system is a spin glass.

A hysteresis loop is clearly observed at 1.8 K, a more distinct magnetization hysteresis loop is observed. It is also noteworthy

that the hysteresis loops along the axis direction exhibit "steps" at the original region due to the effect of weak interchain interactions, indicating a hard-magnetic behavior of **1**.

The magnetic susceptibility of **2** versus temperature was shown in Fig. 10. At 300 K, $\chi_M T$ value of 3.42 cm³ K mol⁻¹ is higher than that for a spin-only case (1.87 cm³ K mol⁻¹, $S = 3/2$) at 300 K, as expected for an orbital contribution. With the lowered temperature, the $\chi_M T$ value keeps decreasing. Such results indicate the presence of antiferromagnetic interaction occurring in cobalt ions in **2**. Fitting the data above 50 K by the Curie–Weiss law gives $C = 4.11$ cm³ K mol⁻¹ and $\theta = -58.80$ K (Fig. 10).

In **3**, the $\chi_M T$ value is 11.02 cm³ K mol⁻¹ per Co3 unit is much larger than the spin value expected for three uncoupled high-spin Co(II) ion (5.65 cm³ K mol⁻¹, $S = 3/2$),[26] revealing a significant orbital contribution. The decrease of the $\chi_M T$ value or the negative θ value can be induced by antiferromagnetic coupling interactions within and between dimeric units as well as strong spin–orbit coupling. When the temperature is decreased, the $\chi_M T$ value increases slightly at ca. 5 K. Fitting the data above 50 K by the Curie–Weiss law gives $C = 13.99$ cm³ K mol⁻¹ and $\theta = -82.02$ K (Fig. 11). The large negative Weiss constant suggests the presence of spin–orbit coupling effect.

At 300 K, a $\chi_M T$ value of 6.67 cm³ K mol⁻¹ is higher than that for a spin-only case (1.87 cm³ K mol⁻¹, $S = 3/2$) in complex **4**. This is also due to the large orbital contribution of Co(II) ion.
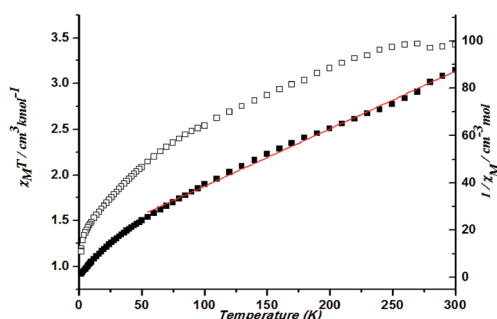

Fig. 10 Plots of $\chi_M T$ vs. T for **2** and the temperature dependence of $1/\chi_M$, the best fit of the curve (red) to the Curie–Weiss law.
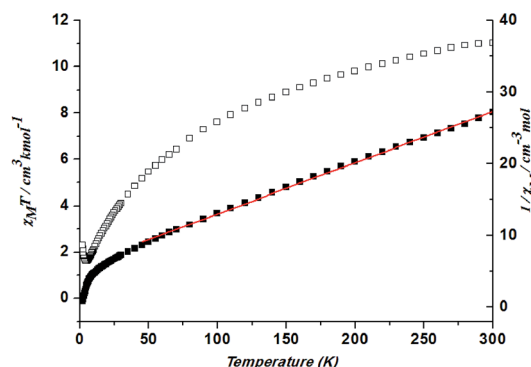

Fig. 11 Plots of $\chi_M T$ vs. T for **3** and the temperature dependence of $1/\chi_M$, the best fit of the curve (red) to the Curie–Weiss law.

Fig. 12 Plots of $\chi_M T$ vs. T for **4** and the temperature dependence of $1/\chi_M$, the best fit of the curve (red) to the Curie–Weiss law.

Fig. 13 Plots of $\chi_M T$ vs. T for **5** and the temperature dependence of $1/\chi_M$, the best fit of the curve (red) to the Curie–Weiss law.
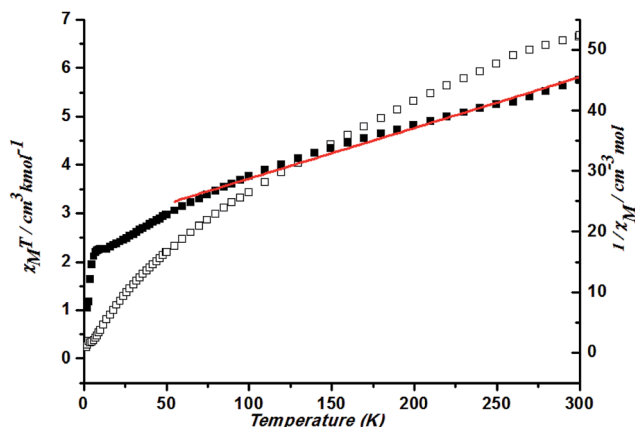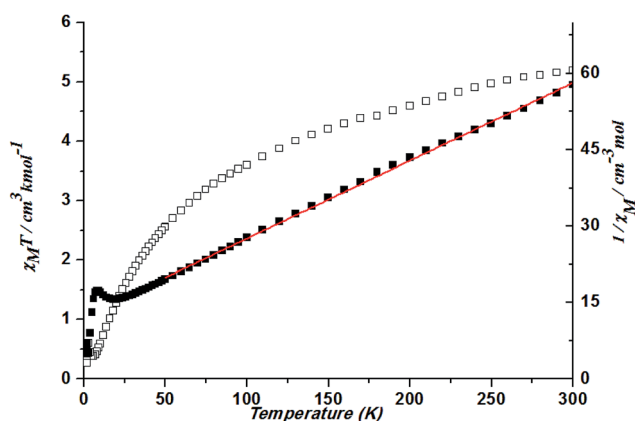
With a decrease in temperature, the $\chi_M T$ keep decreasing. Spin–orbit coupling effects and the presence of possible antiferromagnetic interactions explained the decrease of the $\chi_M T$ plot upon cooling at high temperature. Fitting the data above 50 K by the Curie–Weiss law gives $C = 11.93$ cm^3 K mol^{-1} and $\theta = -242.76$ K (Fig. 12). Such a large value could better be explained by the spin–orbit coupling between Co ions.

At 300 K, a $\chi_M T$ value is 5.19 cm^3 K mol^{-1} in complex **5**. With a decrease in temperature, the $\chi_M T$ decreases gradually and then rapidly. Spin–orbit coupling effects and the presence of possible antiferromagnetic interactions explained the decrease of the $\chi_M T$ plot upon cooling at high temperature. The slow decrease is a typical manner of an orbitally degenerate $^4T_{1g}$ (d$_7$ octahedral) system undergoing spin–orbit coupling. The rapid decrease suggests the possibility of antiferromagnetic coupling. Fitting the data above 50 K by the Curie–Weiss law gives $C = 6.54$ cm^3 K mol^{-1} and $\theta = -80.29$ K (Fig. 13).

4. Conclusion

In this paper, we have demonstrated the formation of five different coordination polymers **1–5** from the solvothermal

reactions of [L]$^-$ with Co(NO$_3$)$_2$, CoCO$_3$, CoCl$_2$, CoSO$_4$. It is noted that the counter anions play an important role in tuning the structural diversities of these frameworks. The crystals of **1–3** could be obtained in one pot and the directed synthesis for each of them was also fulfilled by tuning the ratio between reactants, employing different templates and counter anions. It also confirms the template effect in the synthesis process. The magnetic property investigation reveals that complex **1** exhibits frequency-dependent magnetic behavior.

Conflicts of interest

The authors declare no competing financial interests.

Acknowledgements

References

1 (a) H. Li, B. Zhao, R. Ding, Y. Jia, H. Hou and Y. Fan, *Cryst. Growth Des.*, 2012, **12**, 4170; (b) H. N. Miras, I. Chakraborty and R. G. Raptis, *Chem. Commun.*, 2010, **46**, 2569; (c) Z. F. Wu, B. Tan, Z. H. Deng, Z. L. Xie, J. J. Fu, N. N. Shen and X. Y. Huang, *Eur. J. Inorg. Chem.*, 2016, **22**, 1334; (d) J. F. Ma, J. Yang, G. L. Zheng, L. Li and J. F. Liu, *Inorg. Chem.*, 2003, **42**, 7531.

2 (a) R. J. Li, M. Li, X. P. Zhou, D. Li and M. O'Keeffe, *Chem. Commun.*, 2014, **50**, 4047; (b) D. M. Chen, N. Xu, X. H. Qiu and P. Cheng, *Cryst. Growth Des.*, 2015, **15**, 961; (c) J. Duan, W. Jin and R. Krishna, *Inorg. Chem.*, 2015, **54**, 4279.

3 (a) S. Zhang, J. Ma, X. Zhang, E. Duan and P. Cheng, *Inorg. Chem.*, 2015, **54**, 586; (b) W. Wang, J. Yang, R. Wang, L. Zhang, J. Yu and D. Sun, *Cryst. Growth Des.*, 2015, **15**, 2589.

4 A. Cingolani, S. Galli, N. Masciocchi, L. Pandolfo, C. Pettinari and A. Sironi, *J. Am. Chem. Soc.*, 2005, **127**, 6144.

5 (a) D. Shao, S. L. Zhang, L. Shi, Y. Q. Zhang and X. Y. Wang, *Inorg. Chem.*, 2016, **55**, 10859; (b) C. G. Werncke, M. A. Bouammali, J. Baumard, N. Suaud, C. Martins, N. Guihery, L. Vendier, J. Zheng, J. B. Sortais, C. Darcel, S. Sabo-Etienne, J. P. Sutter, S. Bontemps and C. Pichon, *Inorg. Chem.*, 2016, **55**, 10968; (c) Y. Kim, Y. S. Choi, H. J. Lee, H. Yoon, Y. K. Kim and M. Oh, *Chem. Commun.*, 2014, **50**, 7617; (d) J. Werner, M. Rams, Z. Tomkowicz and C. Näther, *Dalton Trans.*, 2014, **43**, 17333.

6 (a) Y. H. Yu, H. T. Ye, G. F. Hou, C. Y. Ren, J. S. Gao and P. F. Yan, *Cryst. Growth Des.*, 2016, **16**, 5669; (b) H. T. Ye, C. Y. Ren, G. F. Hou, Y. H. Yu, X. Xu, J. S. Gao, P. F. Yan and S. W. Ng, *Cryst. Growth Des.*, 2014, **14**, 3309.

7 B. Chen, Y. Yang, F. Zapata, G. Lin, G. Qian and E. B. Lobkovsky, *Adv. Mater.*, 2007, **19**, 1693.

8 (a) J. F. Ayme, J. Lux, J. P. Sauvage and A. Sour, *Eur. J. Inorg. Chem.*, 2012, **18**, 5565; (b) C. K. Brozek, L. Bellarosa,

T. Soejima, T. V. Clark, N. Lopez and M. Dinca, *Eur. J. Inorg. Chem.*, 2014, **20**, 6871.

9 G. W. Zhou, Y. Z. Lan, F. K. Zheng, X. Zhang, M. H. Lin, G. C. Guo and J. S. Huang, *Chem. Phys. Lett.*, 2006, **426**, 341.

10 (*a*) Q. Yang, X. Chen, Z. Chen, Y. Hao, Y. Li, Q. Lu and H. Zheng, *Chem. Commun.*, 2012, **48**, 10016; (*b*) X. Y. Chen, R. B. Huang, L. S. Zheng and J. Tao, *Inorg. Chem.*, 2014, **53**, 5246.

11 (*a*) F. Zhao, S. Jing, Y. Che and J. Zheng, *CrystEngComm*, 2012, **14**, 4478; (*b*) L. Wang, Z. H. Yan, Z. Xiao, D. Guo, W. Wang and Y. Yang, *CrystEngComm*, 2013, **15**, 5552.

12 (*a*) D. Deng, L. Liu, B. M. Ji, G. Yin and C. Du, *Cryst. Growth Des.*, 2012, **12**, 5338; (*b*) K. P. Rao, M. Higuchi, J. Duan and S. Kitagawa, *Cryst. Growth Des.*, 2013, **13**, 981.

13 (*a*) B. C. Tzeng, Y. C. Hung and G. H. Lee, *Eur. J. Inorg. Chem.*, 2016, **22**, 1522; (*b*) K. Y. Zou, Q. Zou, T. Han, Y. C. Liu, J. J. Wang, X. Zhang and Z. X. Li, *J. Solid State Chem.*, 2016, **235**, 85.

14 (*a*) W. G. Lu, L. Jiang and T. B. Lu, *Cryst. Growth Des.*, 2010, **10**, 4310; (*b*) P. Cui, L. Ren, Z. Chen, H. Hu, B. Zhao, W. Shi and P. Cheng, *Inorg. Chem.*, 2012, **51**, 2303.

15 Z. M. Hao and X. M. Zhang, *Cryst. Growth Des.*, 2007, **7**, 64.

16 (*a*) G. A. Farnum and R. L. LaDuca, *Cryst. Growth Des.*, 2010, **10**, 1897; (*b*) P. Nielsen, H. Toftlund, A. D. Bond, J. F. Boas, J. R. Pilbrow, G. R. Hanson, C. Noble, M. J. Riley, S. M. Neville, B. Moubaraki and K. S. Murray, *Inorg. Chem.*, 2009, **48**, 7033; (*c*) Z. Hulvey, E. Ayala, J. D. Furman, P. M. Forster and A. K. Cheetham, *Cryst. Growth Des.*, 2009, **9**, 4759; (*d*) Y. Y. Liu, J. F. Ma, J. Yang and Z. M. Su, *Inorg. Chem.*, 2007, **46**, 3027; (*e*) L. L. Liu, J. J. Huang, X. L. Wang, G. C. Liu, S. Yang and H. Y. Lin, *Inorg. Chim. Acta*, 2013, **394**, 715.

17 (*a*) R. Seetharaj, P. V. Vandana, P. Arya and S. Mathew, *Arabian J. Chem.*, 2016, DOI: 10.1016/j.arabjc.2016.01.003; (*b*) N. Stock and S. Biswas, *Chem. Rev.*, 2012, **112**, 933; (*c*) T. Yu, S. Wang, X. Li, X. Gao, C. Zhou, J. Cheng, B. Li, J. Li, J. Chang, H. Hou and Z. Liu, *CrystEngComm*, 2016, **18**, 1350.

18 (*a*) B. Ding, P. Yang, Y. Y. Liu, Y. Wang and G. X. Du, *CrystEngComm*, 2013, **15**, 2490; (*b*) B. Ding, Y. Y. Wang, S. X. Liu, X. X. Wu, Z. Z. Zhu, J. Z. Huo and Y. Y. Liu, *CrystEngComm*, 2015, **17**, 5396; (*c*) N. Wang, Y. C. Feng, W. Shi, B. Zhao, P. Cheng, D.-Z. Liao and S.-P. Yan, *CrystEngComm*, 2012, **14**, 2769; (*d*) H. A. Habib, A. Hoffmann, H. A. Hoppe, G. Steinfeld and C. Janiak, *Inorg. Chem.*, 2009, **48**, 2166.

19 (*a*) H. A. Habib, J. Sanchiz and C. Janiak, *Dalton Trans.*, 2008, 1734; (*b*) H. A. Habib, A. Hoffmann, H. A. Hoppe and C. Janiak, *Dalton Trans.*, 2009, 1742; (*c*) X. X. Lv, L. L. Shi, K. Li, B. L. Li and H. Y. Li, *Chem. Commun.*, 2017, **53**, 1860; (*d*) K. Li, X. X. Lv, L. L. Shi, L. Liu, B. L. Li and B. Wu, *Dalton Trans.*, 2016, 15078.

20 (*a*) B. Liu, Y. H. Yu, W. H. Jiang, G. F. Hou and J. S. Gao, *Inorg. Chem. Commun.*, 2015, **54**, 12; (*b*) W. H. Jiang, J. L. Liu, L. Z. Niu, B. Liu, Y. H. Yu, G. F. Hou and D. S. Ma, *Polyhedron*, 2017, **124**, 191.

21 G. M. Sheldrick, Programs for the Solution and Refinement of Crystal Structures, *SHELXS-97*, University of Götingen, Germany, 1997.

22 V. A. Blatov and A. P. Shevchenko, *TOPOS-Version 4.0 professional (beta evaluation)*, Samara State University, Samara, Russia, 2006.

23 P. Mahata, S. Natarajan, P. Panissod and M. Drillon, *J. Am. Chem. Soc.*, 2009, **131**, 10140.

24 (*a*) N. F. Chilton, C. A. Goodwin, D. P. Mills and R. E. Winpenny, *Chem. Commun.*, 2015, **51**, 101; (*b*) D. N. Woodruff, R. E. Winpenny and R. A. Layfield, *Chem. Rev.*, 2013, **113**, 5110; (*c*) J. Zhang, K. Wang, X. Li and E. Gao, *Inorg. Chem.*, 2014, **53**, 9306.

25 (*a*) J. Y. Zhang, K. Wang, X. B. Li and E. Q. Gao, *Inorg. Chem.*, 2014, **53**, 9306; (*b*) J. P. Zhao, Q. Yang, Z. Y. Liu, R. Zhao, B. W. Hu, M. Du, Z. Chang and X. H. Bu, *Chem. Commun.*, 2012, **48**, 6568.

26 (*a*) S. J. Liu, L. Xue, T. L. Hu and X. H. Bu, *Dalton Trans.*, 2012, **41**, 6813; (*b*) X. Z. Song, S. Y. Song, M. Zhu, Z. M. Hao, X. Meng, S. N. Zhao and H. J. Zhang, *Dalton Trans.*, 2013, **42**, 13231.